Applied Surface Science 363 (2016) 113–121

Contents lists available at ScienceDirect

Applied Surface Science

journal homepage: www.elsevier.com/locate/apsusc

Preparation of surface-functionalized porous clay heterostructures *via* carbonization of soft-template and their adsorption performance for toluene

Yuebo Wang[a,b,d], Xiaoli Su[a,b,c], Zhen Xu[e], Ke Wen[a,b,d], Ping Zhang[a,b,d], Jianxi Zhu[a,d,*], Hongping He[a,d]

[a] CAS Key Laboratory of Mineralogy and Metallogeny, Guangzhou Institute of Geochemistry, Chinese Academy of Sciences, Tianhe District, Guangzhou 510640, China
[b] University of Chinese Academy of Sciences, Beijing 100049, China
[c] School of Material Science and Engineering, Jingdezhen Ceramic Institute, Jingdezhen 333001, China
[d] Guangdong Provincial Key Laboratory of Mineral Physics and Materials, 511 Kehua Street, Guangzhou 510640, China
[e] School of Materials Science and Engineering, Central South University, Changsha 410083, China

ARTICLE INFO

Article history:
Received 23 August 2015
Received in revised form
19 November 2015
Accepted 30 November 2015
Available online 7 December 2015

Keywords:
Porous clay heterostructures
Surface functionalization
Adsorption
Affinity
Toluene

ABSTRACT

A new type of surface-functionalized porous clay heterostructures (SF-PCH) was synthesized *via* carbonization of the template agents with sulfuric acid. The converted carbons deposited on the porous surface of the SF-PCH samples and changed their surface chemical properties. The composites possessed a maximum carbon content of 5.35%, a large specific surface area of 428 m^2/g and micropore volume of approximately 0.2 cm^3/g. The layered and porous structure of SF-PCH was retained after carbonization and calcination when sulfuric acid solution with a mild concentration was used. Analysis by XPS confirmed that the carbonaceous matter in the pore channels was functionalized with various organic groups, including carbonaceous, nitrogenous, and sulfated groups. Both the surface chemical property and structural characteristic of adsorbents have effects on the adsorption properties of SF-PCH for toluene. The SF-PCH samples exhibited a stronger adsorption affinity to toluene compared with untreated PCH in the low pressure region, which is more valuable in the practical applications. These results demonstrate that carbonization of soft-template is a feasible process for the surface modification of PCH, enabling the resulting composites to become promising candidates for application in toluene emission control.

1. Introduction

The volatile organic compounds (VOCs) from anthropogenic emission has become a critical component of hazardous air pollutants. Volatile organic compounds have complex composition, and most of them are noxious for environment and human health, such as benzene, toluene, and formaldehyde, which are considered by many authorities to be proven or probable human carcinogens [1,2]. Considering their economic values, hardly complete removal or causing secondary pollution in removal (*e.g.*, combustion method), VOCs have to be trapped and recycled. Adsorption is one of the widely accepted methods for collecting these harmful compounds because of the flexibility of the system, low energy, and inexpensive operation costs [3]. Owing to the following properties, activated carbon is the most common materials used for adsorption of VOCs: highly developed surface area, large pore volumes, low price and wide range of raw material source [4–6]. However, some disadvantages of activated carbon usually encounter in practical gas adsorption, including flammability, pore clog, hygroscopicity, and other problems associated with regeneration [7].

Porous clay heterostructures (PCH) is a kind of pillared interlayered clays (PILC) according to the definition of IUPAC [8]. Because of possessing large surface area, inherent or enhanced solid acidity, and unique combined microporosity and mesoporosity, PCH is a promising candidate for applications as adsorbents [9–11], catalysts [12–14], carriers [15], and templates [16–18]. Compared with

* Corresponding author at: CAS Key Laboratory of Mineralogy and Metallogeny, Guangzhou Institute of Geochemistry, Chinese Academy of Sciences, Tianhe District, Guangzhou 510640, China. Tel.: +86 20 85290181; fax: +86 20 85290181.
E-mail addresses: wangyuebo@gig.ac.cn (Y. Wang), quickly985@163.com (X. Su), 649832777@qq.com (Z. Xu), wenke@gig.ac.cn (K. Wen), zhangp@gig.ac.cn (P. Zhang), zhujx@gig.ac.cn (J. Zhu), hehp@gig.ac.cn (H. He).

http://dx.doi.org/10.1016/j.apsusc.2015.11.261
0169-4332/

microporous PCH, the porous surface modification of macroporous adsorbents (*e.g.*, diatomite) can be relatively easily performed by grafting silane or organophilic zeolite [19,20] to improve their affinity to VOCs without concerning about the blockage of macropores. The pore sizes of PCH distribute in the supermicropore to small mesopore domain. For such small pores, their porous surfaces are hard to be modified and functionalized. The micropores are more likely to become clogged by grafted molecules.

In some previous works focusing on improving the adsorption and catalytic performances of PCH, the native template agents or additional organic species were partially or completely retained to functionalize the internal surface of the porous silica. Depending on the calcination temperature and atmosphere, as well as the composition and concentration of extracting solvents, the surface chemical properties and the solid acidity were tuned through adjusting the contents of organic residues on the internal pore surface. The surface-functionalized materials with residual surfactant in their pores exhibited good hydrophobicity or catalytic activity [21,22]. However, their relatively low thermostability caused by the organic residues hindered the regeneration of the adsorbents. In some other reports, a variety of functional groups (*e.g.*, methyl [23,24], phenyl [25–27], and thiol [28]) were incorporated into the framework through co-condensation methods by introducing silane with specific functional groups during the one-step synthesis of porous materials. The resultant materials exhibited greater thermostability by the greater stability of the Si–C bonds formed between functional groups and pore walls. However, part of the incorporated functional groups remained in the framework, which negatively affected the condensation of silicon species and further affected the crystallinity and the arrangement of pore network.

Recently, a synthesis route for preparing carbon materials from native template agents [29] or other carbon sources [30,31] was applied in the preparation of mesostructured silica–carbon composites. The surfactant in the pore channels was carbonized with the aid of sulfuric acid. Both the silica framework (hard template) and the template agent (soft template) were preserved in this method. The Si-framework and carbonaceous materials in the pores were acid-proof and relatively thermostable, which ensured the mesoporous structural ordering and enhanced the thermostability of the composite. The final products combined the textural characteristics of mesostructured silica and the surface chemical properties of carbon materials [29–31]. Such silica–carbon composites attract attention because of their potential applications in catalysis and liquid-phase adsorption. The suitability of the composites in these applications stems from their good textural and surface chemical properties [32,33], whereas their application for removing VOCs is rarely reported. Surface-functionalized porous silica may exhibit a greater adsorption affinity to VOCs, *e.g.*, toluene, by the incorporation of converted carbon deposited inside the pores of silica. This feature inspires us to make an attempt on fabricating SF-PCH as gas-phase adsorbents for toluene removal.

In this study, we report the preparation of SF-PCH *via* the carbonization of native template agents with H_2SO_4 and the effect of acid concentration on the physicochemical characteristics of SF-PCH. The adsorption performance of SF-PCH was evaluated on the base of the adsorption of toluene. The influence of the structural characteristics and surface chemical properties on the adsorption behaviors was also discussed.

2. Experimental

2.1. Materials

Montmorillonite (Mt) obtained from Inner Mongolia, China, showed the very high purity above 95% containing quartz as an impurity, confirmed by XRD measurement. Its chemical compositions (wt%) are listed in Table 1. The cation exchange capacity (CEC) was 110.5 mmol/100 g measured through $[Co(NH_3)_6]^{3+}$ cation exchanging method [34,35]. Cetyltrimethylammonium bromide (CTAB, approx. 99%) was purchased from Nanjing Robiot Co., Ltd. Dodecanamine (DDA, approx. 98%) was purchased from Sigma-Aldrich chemistry Co., Ltd. Tetraethylorthosilicate (TEOS, chemically pure), hydrogen peroxide (≥30 wt%), Sulfuric acid (95.0–98.0%), hydrofluoric acid (≥40%), hydrochloric acid (36.0–38.0%), and toluene (used as adsorbate in adsorption experiments, ≥99.5%) were purchased from Guangzhou chemical reagent factory.

2.2. Synthesis of SF-PCH samples

The organo-montmorillonite (OMt) was prepared by the exchange of CTA^+, whose amount was 1 time the cation exchange capacity (CEC) of Mt. The dispersion was stirred at 80 °C for 10 h. After filtration, the obtained OMt was washed with distilled water to remove excess water-soluble surfactant. The OMt was air dried at 80 °C and ground sufficiently to pass 100-mesh sieve. Subsequently, OMt was mixed and continuously stirred with DDA and TEOS with the mass ratio of OMt/neutral amine/TEOS of 1/1/120 for 4 h at 60 °C, centrifuged without washing and then air-dried overnight. The same procedure was also performed without OMt to fabricate silica materials as a reference to the PCH samples. The resultant materials are referred to as P-T. The product heated at 550 °C for 6 h in air is named P-air.

The PCH precursor (before calcination) was dispersed in H_2O_2 (solid/liquid = 1 g/100 mL) for 15 h to oxidize the template agents in the pore channels. Subsequently, 2.5 g of the obtained materials were dispersed in H_2SO_4 solutions with a concentration of *x* wt% (*x* = 0, 1, 2, 5, and 10). The dispersion was heated in air at 100 °C for 6 h and then at 160 °C for 12 h. Finally, the resulting gray or black solid was heated at 550 °C for 6 h. The process was under flowing nitrogen. The final product is designated as P/C-*x*H. Particularly, P/C-0H means that no H_2SO_4 was used in the preparation of the corresponding SF-PCH.

To eliminate the influence of the base clay on the characterization of the converted carbon from the surfactant, carbonaceous materials were obtained by dissolving the mineral host and interlayered Si-framework with HF and HCl. The templated carbon obtained from P/C-2H is labeled as C-2H.

2.3. Characterization methods

Major element oxides were analyzed using a Rigaku RIX 2000 X-ray fluorescence spectrometer (XRF) on fused glass beads. Calibration lines used in quantification were produced by bivariate regression of data from 36 reference materials encompassing a wide range of silicate compositions, and analytical uncertainties are mostly between 1% and 5%.

Table 1
Chemical composition of the pristine Mt and P-air.

	SiO_2 (%)	Al_2O_3 (%)	Fe_2O_3 (%)	CaO (%)	MgO (%)	Na_2O (%)	K_2O (%)	MnO (%)	TiO_2 (%)	P_2O_5 (%)	L.O.I. (%)
Mt	58.16	16.95	5.26	2.29	3.57	0.19	0.15	0.03	0.20	0.08	13.12
P-air	80.06	7.75	2.74	0.08	2.38	0.05	0.09	0.02	0.18	0.01	6.97

The CHN elemental analysis was performed using an Elementar Vario EL III Universal CHNOS Elemental Analyzer.

X-ray diffraction (XRD) patterns were obtained using a Bruker D8 Advance diffractometer with a Ni filter and Cu Kα radiation (λ = 0.154 nm) generated at 40 kV and 40 mA. The scan rate was 2° (2θ)/min.

High resolution transmission electron micrographs were obtained on a JEM 2010 (HR) transmission electron microscope (TEM). Samples were prepared by depositing diluted clay mineral dispersions (100 mg/L) onto a copper mesh grid.

Nitrogen adsorption/desorption isotherms were measured at −196 °C using a Micromeritics ASAP 2020 instrument. Prior to analysis, samples were outgassed at 120 °C for 12 h. The specific surface area was calculated by the BET equation and the total pore volume was evaluated from nitrogen uptake at a relative pressure (p/p_0) of 0.97 [36]. The t-method was used to calculate the microporous specific surface area, external specific surface area, and micropore volume [37]. The pore size distributions (PSD) of PCH are in the range of the transition between micro and mesopores. The non-local density functional theory (NLDFT) method, which can be applied across the complete micropore–mesopore range [38], was used to carry out the PSD analysis [39].

Fourier-transform infrared spectroscopy (FTIR) spectra of the samples were measured by a Bruker Vertex-70 Fourier-transform infrared spectrometer using KBr pellets in transmission mode at a resolution of 2 cm^{-1} over 64 scans collection.

X-ray photoelectron spectroscopy (XPS) analysis was carried out by using a Thermo Scientific Escalab 250 instrument, equipped with monochromatic Al Kα (10 mA, 14 kV). All binding energies were referenced to the C1*s* hydrocarbon peak at 284.8 eV.

2.4. Adsorption measurement of toluene

The Intelligent Gravimetric Analyser (IGA-003, Hiden Isochema Instrument) was used to measure the adsorption isotherms of toluene. To guarantee removal of the excess water and impurities on micropores, the samples (approximately 50 mg for each run) in the vessel of IGA-003 were vacuumed up to 10^{-5} Pa and outgassed at 120 °C for 12 h before the measurements. The adsorption experiments were carried out at a temperature of 25 °C.

3. Results and discussion

3.1. Physicochemical properties of SF-PCH

Depending on the variation of acid concentration, the carbon content (f_C) in the SF-PCH samples varied within the range from 1.95 to 5.35 wt%, as summarized in Table 2. Compared to the PCH samples calcined in air (P-air) and in N_2 without acid treatment (P/C-0H), the acid modification substantially increased the amount of carbon. However, the solution with greater acid concentrations led to a decrease of f_C because of the partial gasification of carbon by SO_3 produced *in situ* ($SO_3 + C \rightarrow SO_2 + CO/CO_2$) [29,40]. Therefore, it is crucial to pretreat the PCH precursor with H_2SO_4 to obtain the higher carbon amount in the resulting material. An H_2SO_4 solution with moderate concentration is required for better preservation of carbon.

Table 2
Total carbon, nitrogen, and sulfur contents of the PCH samples.

Samples	f_C (by mass, %)	f_N (by mass, %)	f_S (by mass, %)
P-air	<0.01	<0.01	<0.01
P/C-0H	0.73	0.10	<0.01
P/C-1H	3.47	0.11	0.14
P/C-2H	5.35	0.16	0.34
P/C-5H	4.59	0.19	0.93
P/C-10H	1.95	0.16	0.54

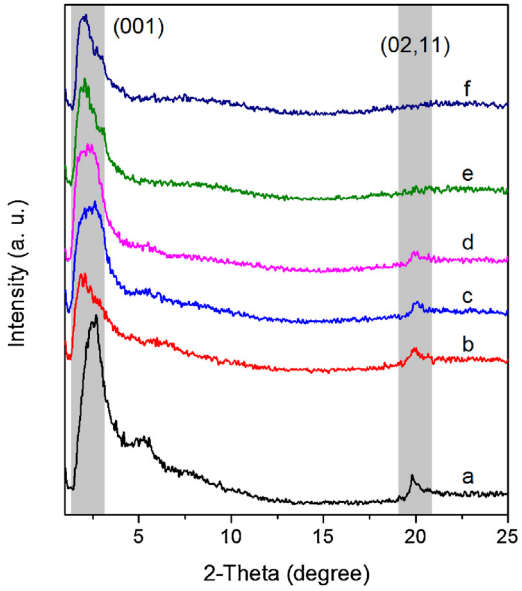

Fig. 1. XRD patterns of the PCH samples: (a) P-air, (b) P/C-0H, (c) P/C-1H, (d) P/C-2H, (e) P/C-5H, and (f) P/C-10H.

The increase in the acid concentration also affected the degree of crystallization of the SF-PCH. Acid treatment of clay minerals with a strong inorganic acid resulted in solid products that contained unaltered layers and amorphous three-dimensional cross-linked silica, depending on the extent of acid activation [41]. As for the PCH samples, sample P-air without acid modification exhibited a well-resolved and intense basal spacing (Fig. 1a). Although the bulky CTA^+ cations in PCH precursor hindered the access of protons (H^+ ions) to the layers and thus protected the base clay from degradation in acid [42], the plate-like particles of PCH were still partially disintegrated by acid attack during the heat treatment (Fig. 1c–f). The patterns of the SF-PCH samples showed broader and less intense (0 0 1) reflections because of the disruption of base clay in the acid treatment. The intensities of the characterized non-basal reflections (*hk*-band groups) of Mt, (02,11) at approximately 2θ = 20°, gradually weakened with increasing acid concentration. The (02,11) band even completely disappeared when the acid concentration was 10%, which indicated that the clay hosts were seriously destroyed by the extreme acid.

The morphologies of PCH samples are shown in Fig. 2. The layered structures of P-air, P/C-1H, and P/C-2H were relatively well retained (Fig. 2A–C) with the similar *d*001-values to the results of XRD (>3 nm), respectively. With the increase of the concentration of H_2SO_4 solutions, the layered structures of the SF-PCH samples were progressively destroyed accompanying with the reduction of order degree of layer stacking. The basal spacing of P/C-5H distributed in a wider range compared with P/C-1H and P/C-2H. The layered structure can even hardly be observed in P/C-10H (Fig. 2E) suggesting its structure was thoroughly disrupted with such concentrated acid.

The structural changes of SF-PCH are revealed in their textural properties as well. The acid treatment resulted in a notable decrease of the textural parameters of the SF-PCH samples, including the specific surface area (S_{BET}), microporous specific surface area (S_{micro}), total porous volume (V_{total}), and the micropore volume (V_{micro}), as listed in Table 3. Although the free silica generated during the treatment with more concentrated acid solutions has a very important contribution to the S_{BET} of dissolved samples compared with that of the original Mt [43], the blockage of carbonaceous materials in the two-dimensional pore channels, the destruction of

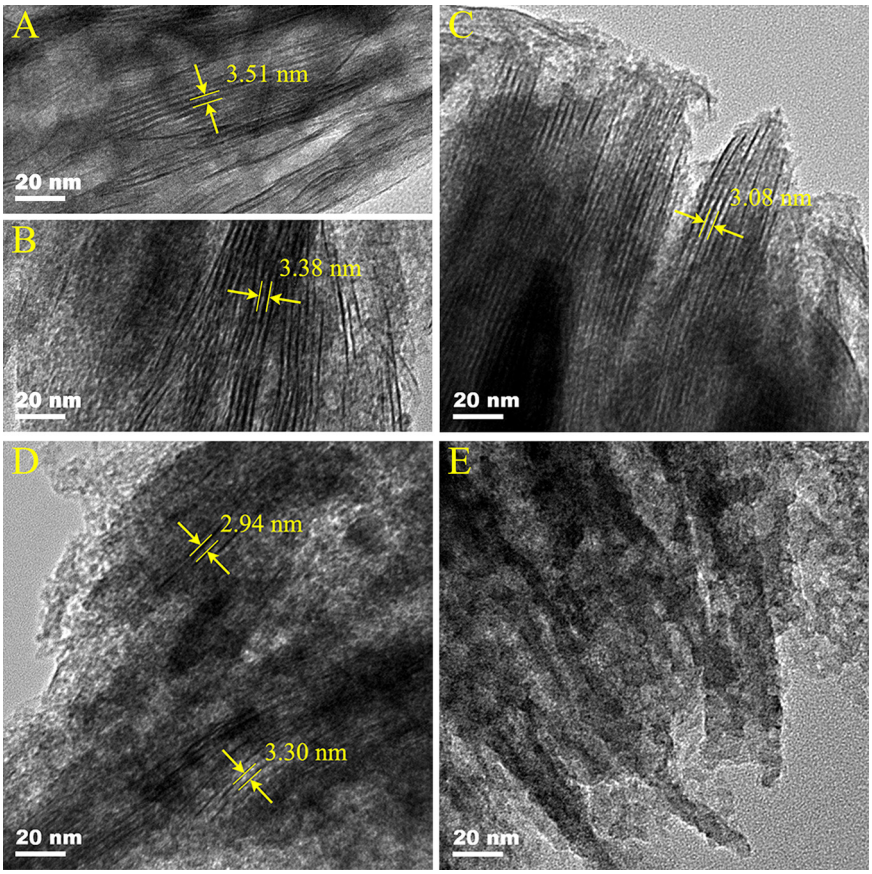

Fig. 2. TEM images of the PCH samples: (A) P-air, (B) P/C-1H, (C) P/C-2H, (D) P/C-5H, and (E) P/C-10H.

the silicate layer, and the partial deintercalation of amorphous silica within the interlayer offset the less positive effect. As a result, the major textural parameters of the SF-PCH samples decreased. The reduction of textural parameters is incongruent with the objective of producing SF-PCH that retain most of their textural properties for VOCs removal. The gradual decreases of S_{BET}, S_{micro}, and V_{micro} of SF-PCH samples with the increase of acid concentration reflected the destruction of base clay by the acid treatment. The smaller textural parameters of P/C-0H compared with the samples with acid treatment suggested that the carbonaceous materials in P/C-0H clogged the pore channels. That was, the acidification contributed to the carbonization of surfactants and to form carbon coating covering the porous surface of SF-PCH. The abnormal increase of V_{total} of P/C-5H and P/C-10H was attributed to the increase in mesopores and macropores from the corrosion of the base clay by acid. N_2 adsorption–desorption isotherms and pore size distributions (PSD) for the PCH samples are shown in Figs. 3 and 4, respectively. The curves for the PCH samples are of type IV with an H3 hysteresis loop, characteristic of plate materials possessing non-rigid slit-like pores according to the IUPAC classification [44]. The mixed characteristics of type I and IV for the curve of P-air were the most probable consequence of the pore sizes being in the transition range from micropores to mesopores [45]. The mixed characteristics, however, were progressively weakened by increasing the acid concentration. The weakened mixed characteristics appeared as the decrease in N_2 adsorption quantity at low p/p_0 and as the increase of the y-axis values at high p/p_0, indicating a decrease of micropore volume and an increase of mesopore volume. The obvious hysteresis loops of P/C-10H also illustrated the increased quantity of mesopores [46], which was consistent with the largest average pore diameter (APD). Furthermore, the PSD of the SF-PCH samples became more distributed than that of the sample P-air (Fig. 4). Their most probable pore sizes (MPPS) gradually decreased from 1.5 nm for P/C-1H to 1.1 nm for P/C-5H with increasing the acid concentration. The micropores were substantially reduced and the mesopores gained on importance eventually when the acid concentration reached 10%. The acid modification may cause partial deintercation of the porous silica from the interlayer spacing. The separation created

Table 3
The textural characteristics of the PCH samples.

Sample	S_{BET} ($m^2\ g^{-1}$)	S_{micro}[a] ($m^2\ g^{-1}$)	$S_{external}$[b] ($m^2\ g^{-1}$)	V_{total}[c] ($cm^3\ g^{-1}$)	V_{micro}[a] ($cm^3\ g^{-1}$)	APD (nm)
P-air	690	456	234	0.550	0.187	3.2
P/C-0H	413	190	223	0.468	0.074	4.5
P/C-1H	469	307	163	0.428	0.128	3.7
P/C-2H	428	258	170	0.390	0.104	3.6
P/C-5H	402	42	360	0.436	0.001	4.3
P/C-10H	316	0	316	0.541	0	6.8

[a] From t-method.
[b] $S_{external} = S_{BET} - S_{micro}$.
[c] From the amount adsorbed at the relative pressure of 0.97.

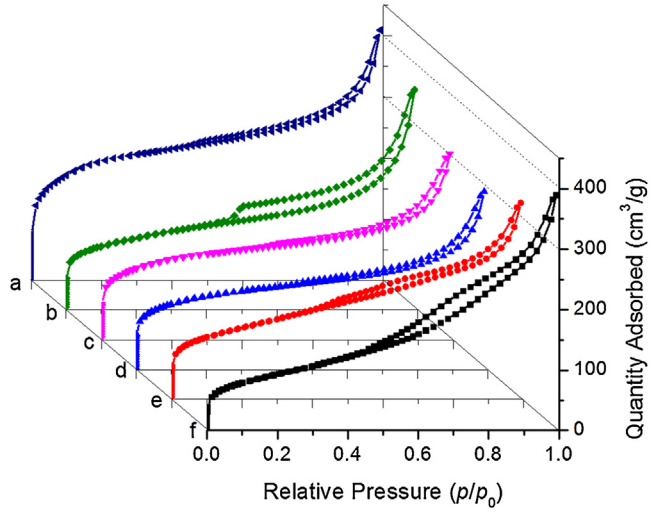

Fig. 3. Nitrogen adsorption/desorption isotherms at −196 °C for the PCH samples: (a) P-air, (b) P/C-0H, (c) P/C-1H, (d) P/C-2H, (e) P/C-5H, and (f) P/C-10H.

vacant spaces larger than the pores in the framework, which promoted the formation of mesopores and macropores [23]. The serious destruction of the base clay by the high-concentration acid led to an increase of mesopore and macropore volume as well [47].

The IR spectroscopy sensitively detects the change of the PCH in the structure and bonding within molecule or crystal [48]. To specify the contribution from the mineral host and the Si-framework generated by TEOS polymerization, the P–T samples were also analyzed. Fig. 5 shows the FTIR spectrum of the PCH samples together with those of Mt, PCH precursor, and P–T. The frequency and assignment of each vibration observed are listed in Table 4. By contrast with the hydroxyl stretching bands in the spectrum of Mt, those in the spectrum of P-air are not separated. The spectrum of P-air contains only one complex band centering at 3435 cm^{-1} due to the incorporation of amorphous silica within the interlayer. For the same reason, the Si–O asymmetric stretching vibration and the Si–O–Si deformation vibration exhibit upward shifts to 1066 and 468 cm^{-1}, respectively. The presence of absorption bands appear at 2927, 2855, 1489 and 1473 cm^{-1} in the spectrum of PCH precursor (Fig. 5h) demonstrates the surfactant used as the template exists in the sample. However, these bands are no longer observed in PCH samples, indicating the surfactant is completely removed or converted into other matter such as carbon. The bands in the spectrum of Mt in the range 915–518 cm^{-1} disappear as a consequence of the release of these less-stable OH groups, which are mainly connected to both aluminium and magnesium, during calcination [48]. For the SF-PCH samples, the chemical character of P–T induced by acid modification becomes more obvious and is observable in three regions of their spectra. The band near 1066 cm^{-1} (ν_{as}Si–O) in the spectrum of P-air progressively moves to 1071 cm^{-1}, then to 1088 cm^{-1} and finally to 1093 cm^{-1}. The shoulders at approximately 970 cm^{-1} (νSi–OH) and 563 cm^{-1} (silica ring or cyclic structure vibration) of P-air, respectively, grow into well-resolved bands in the spectrum of P/C-10H. The three changes

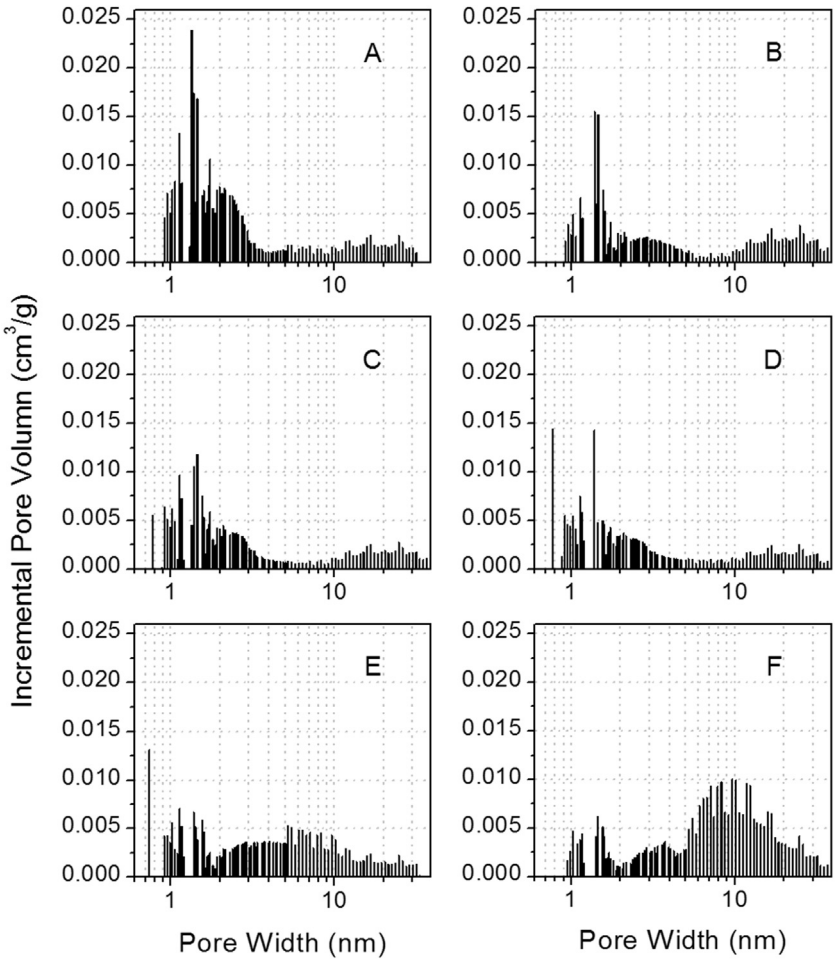

Fig. 4. Pore size distribution patterns for the PCH samples: (A) P-air, (B) P/C-0H, (C) P/C-1H, (D) P/C-2H, (E) P/C-5H, and (F) P/C-10H.

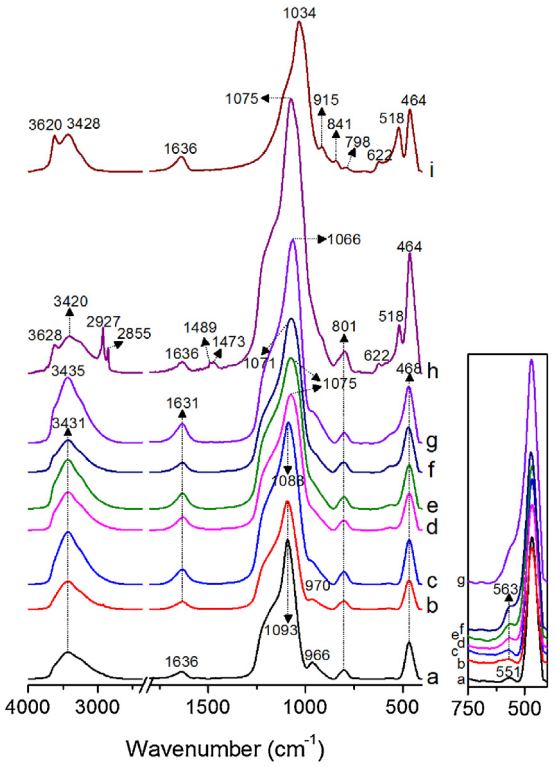

Fig. 5. FTIR spectra of (a) P-T, (b) P/C-10H, (c) P/C-5H, (d) P/C-2H, (e) P/C-1H, (f) P/C-0H, (g) P-air, (h) PCH precursor, and (i) Mt. The inset shows the corresponding spectra in the range from 750 to 400 cm^{-1}.

in the spectra of acid-treated samples were mainly attributed to the different anti-acid performances between exterior clay layers and incorporated amorphous silica pillars. The surface chemical properties of the non-acid resistant Mt can be changed by H_2SO_4 attack [49]. In contrast, polycondensation of the acid-proof polysiloxane-like compounds from TEOS can be further performed after the surfactant has been removed [23]. Therefore, the spectra of the SF-PCH samples become more like that of P–T.

XPS was used to characterize the functional groups on the surface of carbonaceous matter in the pores of the Si-framework. Fig. 6 shows the C 1*s*, O 1*s*, N 1*s*, and S 2*p* core-level spectra of C-2H and their peak-fitting envelopes. Three peaks were deconvolved in the C 1*s* spectrum presented in Fig. 6A. The peak at 284.7 eV corresponded to carbon in aromatic and aliphatic structures, the peak at 285.6 eV to C–O– in phenolic, alcoholic or etheric structures, and the last one at 288.0 eV to C═O in carbonyl or quinone [33,53]. The O 1*s* spectrum confirmed the presence of these oxygenated groups. Thus, deconvolution of the O 1*s* spectrum (Fig. 6B) yielded the peaks corresponding to oxygen doubly bonded to carbon at 531.5 eV and the peak corresponding to oxygen singly bonded to carbon in hydroxyl groups or organic groups (*i.e.*, aromatic rings, phenols or ethers) at 532.8 eV [54]. The N 1*s* signal (Fig. 6C) was fitted by three individual peaks. The main peak at 399.8 eV and two shoulders at 398.2 and 401.2 eV were attributed to pyrrolic groups, pyridinic groups, and quaternary nitrogen, respectively [30,55]. The nitrogen in quaternary ammonium cations was predominantly converted into pyrrolic groups, which was likely caused by the relatively low calcination temperature [56]. Lastly, the S 2*p* signal (Fig. 6D) was split into four peaks. The unresolved doublets at 163.8 and 165.1 eV (S $2p_{3/2}$ and S $2p_{1/2}$) corresponded to the carbon forming sulfide bridges (–C–S–C–), whereas another doublets at 167.7 and 169.0 eV (S $2p_{3/2}$ and S $2p_{1/2}$) were related to the sulfonyl bridges (–C–SO_2–C–) [30,57]. Most of the sulfonyl bridges were formed through the dehydration of sulfonic groups during pyrolysis and were transformed into sulfide bridges [58]. Consequently, a sulfide/sulfonyl ratio of 7.0 for C-2H was obtained as estimated by XPS analysis. The deconvolution of the S 2*p* signal shown that H_2SO_4 was associated with both dehydration reactions and the formation of sulfonic groups during the carbonization reaction. The dehydration process aromatized organic templates, while the sulfonating procedure increased the yield of carbonaceous residue because of the cross-linking process that occurred through the formation of sulfide and sulfonyl bridges between adjacent phenyl rings [58].

An illustration of the synthesis route for SF-PCH is presented in Fig. 7. The synthesis scheme mainly involves two steps: (a) the preparation of as-synthesized PCH samples without removing the template agents and (b) carbonization of the template agents through acid and heat treatments. The converted carbonaceous materials are dispersed in the two-dimensional pores of the Si-framework within the interlayer. The obtained results revealed the successful incorporation of various functional groups into the composites.

3.2. Toluene adsorption performances of SF-PCH

The toluene adsorption experiments of the SF-PCH samples as well as P-air were carried out and their adsorption isotherms are shown in Fig. 8. In the low pressure region, the amount adsorbed increased linearly with pressure. The interaction between adsorbed molecules can be neglected and the adsorbent–adsorbate interactions dominate in adsorption process (*i.e.*, monolayer coverage) [59]. The Henry's law [45,59] is used to fit the adsorption data in $p/p_0 < 0.06$ (the area in the dashed rectangle in Fig. 8), and the equation is described as follow:

$$q = H \times \frac{p}{p_0}$$

where q (mg/g) is the amount of the adsorbed toluene at the relative pressure p/p_0 and H (10^3 mg/g) is the Henry constant, which reflects the adsorption affinity between the probe molecule and the porous surface. As shown in Table 5, the H values of all the SF-PCH samples were significantly larger than that of P-air, indicating the stronger adsorption affinity between the toluene molecules and the porous surface of the formers compared with the latter. However, the S_{micro} and V_{micro} of the SF-PCH samples were smaller than those of P-air (Table 3). The paradoxically larger amounts of the adsorbed toluene

Table 4
The assignments of the FTIR vibrations shown in Fig. 5 [48,50–52].

Position (cm^{-1})	Assignments	Position (cm^{-1})	Assignments
3628, 3620	OH stretching of structural hydroxyl groups	970, 966	Si–OH stretching
3435, 3431, 3428, 3420	OH stretching of water	915	Al–Al–OH deformation
2927	CH_2 asymmetric stretching	841	Al–Mg–OH deformation
2855	CH_2 symmetric stretching	801, 798	Si–O stretching of silica
1636, 1631	OH deformation of water	622	Coupled Al–O and Si–O, out-of-plane bending
1489	C–H symmetrical bending of N^+-CH_3	563, 551	Silica ring or cyclic structure vibration
1473	CH_2 deformation (scissoring)	518	Al–O–Si deformation
1093, 1088, 1075, 1066, 1034	Si–O stretching	468, 464	Si–O–Si deformation

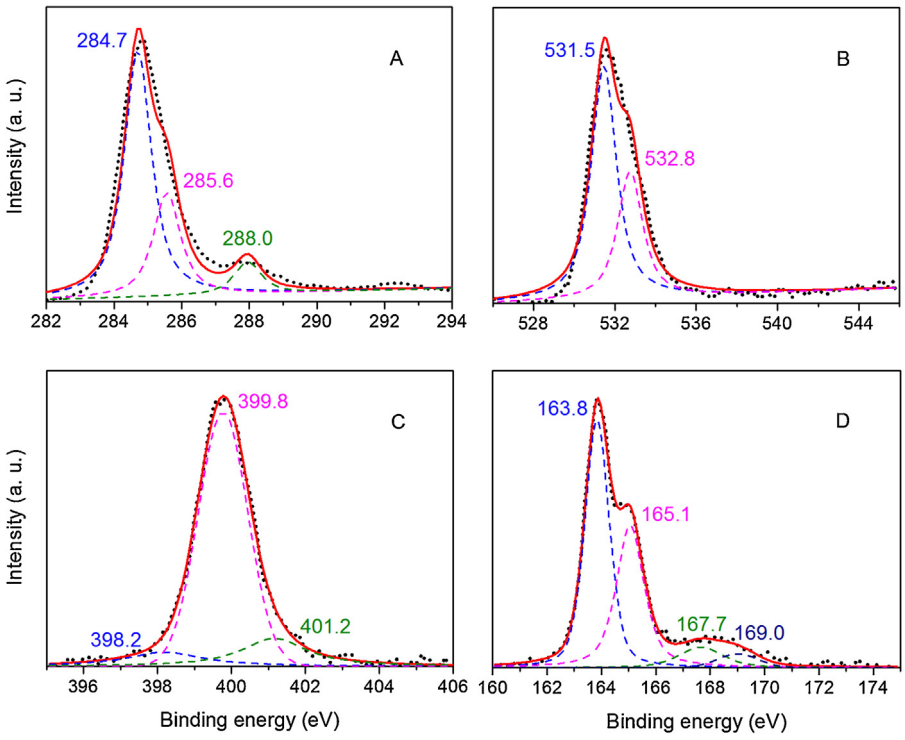

Fig. 6. (A) C 1*s*, (B) O 1*s*, (C) N 1*s*, and (D) S 2*p* XPS spectra for the carbonaceous material from P/C-2H.

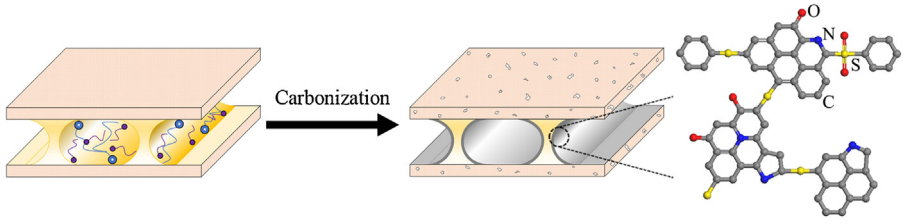

Fig. 7. Illustration of the fabrication of SF-PCH.

of SF-PCH in the low pressure region were mainly attributed to the carbonaceous materials in the pore channels. The carbon coating on the siliceous surface of porous framework led to the decreased MPPS of SF-PCH. The decreased micropores has a larger adsorption potential to adsorbate. On the other hand, among the SF-PCH samples, the largest quantity adsorbed of toluene (P/C-2H) corresponded to the largest f_C (Table 2). The result suggested that the carbonaceous surface within interlayer improved the adsorption affinity to toluene compared with siliceous surface. With the increase of concentration of acid, the porous structure of SF-PCH was gradually destroyed. The extreme destruction of the porous structure of P/C-5H and P/C-10H led to the smaller adsorption amounts to toluene though their f_C were larger than that of P/C-1H.

In the high pressure ranges, the adsorption capacity of toluene for P-air grew higher than those of the SF-PCH samples with the increase of partial pressure. The variation of equilibrium adsorption capacity of PCH for toluene (q_e) (Table 5) was in accordance with the variation of their V_{total} (Table 3). By contrast with low pressure region, multilayer adsorption occurs in the high pressure

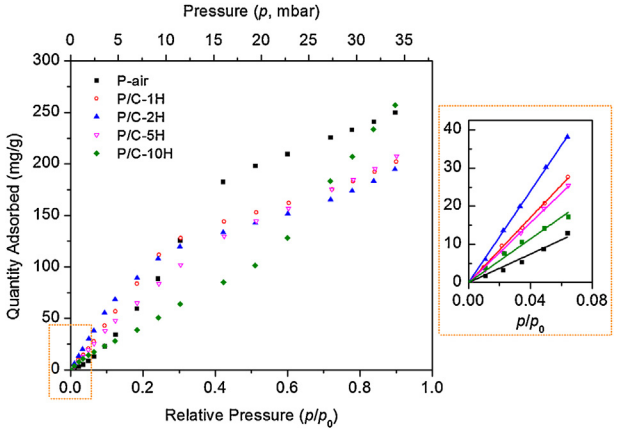

Fig. 8. Adsorption isotherms for toluene of P-air, P/C-1H, P/C-2H, P/C-5H, and P/C-10H (solid lines for simulated based on Henry's law equation).

Table 5
Equilibrium adsorption capacities and Henry modal parameters for toluene on the PCH samples.

Samples	Equilibrium adsorption capacities q_e (mg/g)	Model parameters	
		Henry constants H (10^3 mg/g)	R^2
P-air	250.0	0.186	0.971
P/C-1H	202.2	0.425	0.998
P/C-2H	194.8	0.599	0.999
P/C-5H	207.7	0.390	0.996
P/C-10H	257.2	0.285	0.981

region and the adsorbate–adsorbate interactions become more prevalent in the high pressure region [9,59]. Accordingly, the same variations of q_e and V_{total} stemmed from the change of porous structure of PCH. The different changing trend of quantity adsorbed to toluene between low and high pressure region indicated that both the surface chemical property and structural characteristic of adsorbents affected their adsorptive performance to adsorbate. The SF-PCH samples prepared with moderate carbonization conditions combined the textural characteristics of porous PCH and surface chemical properties of carbon materials.

Notably, in most industrial environments and homes, the pollutants are present in very dilute streams [60]. The VOCs harm human health even at very low concentration [1]. Consequently, the higher adsorption capacities for P/C-1H and P/C-2H in the low pressure region compared with P-air are more meaningful in the practical applications.

4. Conclusions

We have reported a synthetic procedure for fabricating surface-functionalized porous clay heterostructures. The synthetic strategy employed template agents as the carbon source. After treatment with H_2SO_4 solutions with different concentrations and calcination under N_2 at 550 °C, the template agents were converted into amorphous carbon and covered the porous surface of SF-PCH. By contrast with the f_C of P-air, the f_C of SF-PCH substantially increased and reached a maximum of 5.35%. The crystallization degree of the materials was disrupted to various degrees depending on the acid concentration. The textural analysis revealed a large specific surface area of 428 m^2/g and a micropore volume of approximately 0.2 cm^3/g for the SF-PCH samples treated with a mild acid solution. XPS analysis confirmed the presence of carbonaceous (aromatic, aliphatic; phenolic, alcoholic, etheric; carbonyl, quinone), nitrogenous (pyridinic, pyrrolic, quaternary nitrogen), and sulfurated groups (thiol, bridging sulfides, bridging sulfones), which were introduced onto the surface of the carbonaceous matter in pores.

By the surface functionalization, the SF-PCH samples exhibited a stronger adsorption affinity to toluene compared with P-air in the low pressure region due to the decreased pore size and the carbon coating on the siliceous surface of porous framework. Both the surface chemical property and structural characteristic of adsorbents have effects on their adsorption properties. The higher adsorption capacities of SF-PCH to toluene in the low pressure region are more valuable when applied in practice. Thus, SF-PCH can be regarded as a good adsorbent for toluene.

Acknowledgments

Supported by the Strategic Priority Research Program of the Chinese Academy of Sciences (Grant No. XDB05050200), CAS/SAFEA International Partnership Program for Creative Research Teams (Grant No. 20140491534), Team Project of Natural Science Foundation of Guangdong Province, China (Grant No. S2013030014241), and the National Natural Science Foundation of China (Grant Nos. 41272060, 41402038). The authors also thank Wenbin Yu, Weiwei Yuan, and Peng Liu for the valuable discussions. This is a contribution (No. IS-2167) from GIGCAS.

References

[1] V.J. Cogliano, Y. Grosse, R.A. Baan, K. Straif, M.B. Secretan, F. El Ghissassi, W.G.V. 88, Meeting report: summary of IARC monographs on formaldehyde, 2-butoxyethanol, and 1-tert-butoxy-2-propanol, Environ. Health Perspect. 113 (2005) 1205–1208.
[2] G. Mastrangelo, E. Fadda, V. Marzia, Polycyclic aromatic hydrocarbons and cancer in man, Environ. Health Perspect. 104 (1996) 1166–1170.
[3] H.N. Wang, M. Tang, K. Zhang, D.F. Cai, W.Q. Huang, R.Y. Chen, C.Z. Yu, Functionalized hollow siliceous spheres for VOCs removal with high efficiency and stability, J. Hazard. Mater. 268 (2014) 115–123.
[4] M.A. Lillo-Rodenas, D. Cazorla-Amoros, A. Linares-Solano, Behaviour of activated carbons with different pore size distributions and surface oxygen groups for benzene and toluene adsorption at low concentrations, Carbon 43 (2005) 1758–1767.
[5] S.J.T. Pollard, G.D. Fowler, C.J. Sollars, R. Perry, Low-cost adsorbents for waste and wastewater treatment: a review, Sci. Total Environ. 116 (1992) 31–52.
[6] N. Mohan, G.K. Kannan, S. Upendra, R. Subha, N.S. Kumar, Breakthrough of toluene vapours in granular activated carbon filled packed bed reactor, J. Hazard. Mater. 168 (2009) 777–781.
[7] X.S. Zhao, Q. Ma, G.Q.M. Lu, VOC removal: Comparison of MCM-41 with hydrophobic zeolites and activated carbon, Energy Fuel 12 (1998) 1051–1054.
[8] R.A. Schoonheydt, T. Pinnavaia, G. Lagaly, N. Gangas, Pillared clays and pillared layered solids (Technical Report), Pure Appl. Chem. 71 (1999) 2367–2371.
[9] F. Qu, L.Z. Zhu, K. Yang, Adsorption behaviors of volatile organic compounds (VOCs) on porous clay heterostructures (PCH), J. Hazard. Mater. 170 (2009) 7–12.
[10] L.Z. Zhu, S.L. Tian, Y. Shi, Adsorption of volatile organic compounds onto porous clay hetero structures based on spent organobentonites, Clay Clay Miner. 53 (2005) 123–136.
[11] C.D. Nunes, J. Pires, A.P. Carvalho, M.J. Calhorda, P. Ferreira, Synthesis and characterisation of organo-silica hydrophobic clay hetero structures for volatile organic compounds removal, Micropor. Mesopor. Mater. 111 (2008) 612–619.
[12] M. Zimowska, H. Palkova, J. Madejova, R. Dula, K. Pamin, Z. Olejniczak, B. Gil, E.M. Serwicka, Laponite-derived porous clay heterostructures: III. The effect of alumination, Micropor. Mesopor. Mater. 175 (2013) 67–75.
[13] M. Munoz, G. Sathicq, G. Romanelli, S. Hernandez, C.I. Cabello, I.L. Botto, M. Capron, Porous modified bentonite as efficient and selective catalyst in the synthesis of 1,5-benzodiazepines, J. Porous Mater. 20 (2013) 65–73.
[14] L. Chmielarz, Z. Piwowarska, P. Kustrowski, A. Wegrzyn, B. Gil, A. Kowalczyk, B. Dudek, R. Dziembaj, M. Michalik, Comparison study of titania pillared interlayered clays and porous clay heterostructures modified with copper and iron as catalysts of the DeNOx process, Appl. Clay Sci. 53 (2011) 164–173.
[15] N. Bunnak, S. Ummartyotin, P. Laoratanakul, A.S. Bhalla, H. Manuspiya, Synthesis and characterization of magnetic porous clay heterostructure, J. Porous Mater. 21 (2014) 1–8.
[16] C. Santos, M. Andrade, A.L. Vieira, A. Martins, J. Pires, C. Freire, A.P. Carvalho, Templated synthesis of carbon materials mediated by porous clay heterostructures, Carbon 48 (2010) 4049–4056.
[17] D. Nguyen-Thanh, T.J. Bandosz, Metal-loaded carbonaceous adsorbents templated from porous clay heterostructures, Micropor. Mesopor. Mater. 92 (2006) 47–55.
[18] Z.B. Wu, J.C. Tian, Z.M. Liu, P. Tian, L. Xu, Y. Yang, Y.Y. Zhang, X.H. Bao, X.M. Liu, X.C. Liu, Template-assisted syntheses of porous metal methylphosphonates, J. Porous Mater. 13 (2006) 73–80.
[19] W. Yu, L. Deng, P. Yuan, D. Liu, W. Yuan, P. Liu, H. He, Z. Li, F. Chen, Surface silylation of natural mesoporous/macroporous diatomite for adsorption of benzene, J. Colloid Interf. Sci. 448 (2015) 545–552.
[20] W.B. Yu, L.L. Deng, P. Yuan, D. Liu, W.W. Yuan, F.R. Chen, Preparation of hierarchically porous diatomite/MFI-type zeolite composites and their performance for benzene adsorption: the effects of desilication, Chem. Eng. J. 270 (2015) 450–458.
[21] L. Huang, Q.L. Huang, H.N. Xiao, M. Eic, Effect of cationic template on the adsorption of aromatic compounds in MCM-41, Micropor. Mesopor. Mater. 98 (2007) 330–338.
[22] S. Sumiya, Y. Kubota, Y. Oumi, M. Sadakane, T. Sano, Mesoporous silicas containing carboxylic acid: preparation, thermal degradation, and catalytic performance, Appl. Catal. a-Gen. 372 (2010) 82–89.
[23] R. Ishii, M. Nakatsuji, K. Ooi, Preparation of highly porous silica nanocomposites from clay mineral: a new approach using pillaring method combined with selective leaching, Micropor. Mesopor. Mater. 79 (2005) 111–119.
[24] M. Nakatsuji, R. Ishii, Z.M. Wang, K. Ooi, Preparation of porous clay minerals with organic–inorganic hybrid pillars using solvent-extraction route, J. Colloid Interf. Sci. 272 (2004) 158–166.
[25] L.M. Wei, T. Tang, B.T. Huang, Novel acidic porous clay heterostructure with highly ordered organic–inorganic hybrid structure: one-pot synthesis of mesoporous organosilica in the galleries of clay, Micropor. Mesopor. Mater. 67 (2004) 175–179.
[26] M.L. Pinto, J. Pires, J. Rocha, Porous materials prepared from clays for the upgrade of landfill gas, J. Phys. Chem. C 112 (2008) 14394–14402.
[27] H.H. Mao, X.X. Gao, J.H. Yang, B.S. Li, A novel one-step synthesis of mesostructured silica-pillared clay with highly ordered gallery organic-inorganic hybrid frame, Appl. Surf. Sci. 257 (2011) 4655–4662.
[28] A.J. Tchinda, E. Ngameni, I.T. Kenfack, A. Walcarius, One-step preparation of thiol-functionalized porous clay heterostructures: application to Hg(II) binding and characterization of mass transport issues, Chem. Mater. 21 (2009) 4111–4121.
[29] P. Valle-Vigon, M. Sevilla, A.B. Fuertes, Mesostructured silica-carbon composites synthesized by employing surfactants as carbon source, Micropor. Mesopor. Mater. 134 (2010) 165–174.
[30] P. Valle-Vigon, M. Sevilla, A.B. Fuertes, Functionalization of mesostructured silica-carbon composites, Mater. Chem. Phys. 139 (2013) 281–289.

[31] B. Du, X. Zhang, L.L. Lou, Y.L. Dong, G.X. Liu, S.X. Liu, Synthesis of acid-functionalized composite via surface deposition of acid-containing amorphous carbon, Appl. Surf. Sci. 258 (2012) 7166–7173.
[32] P. Valle-Vigon, M. Sevilla, A.B. Fuertes, Sulfonated mesoporous silica-carbon composites and their use as solid acid catalysts, Appl. Surf. Sci. 261 (2012) 574–583.
[33] P. Valle-Vigon, M. Sevilla, A.B. Fuertes, Carboxyl-functionalized mesoporous silica-carbon composites as highly efficient adsorbents in liquid phase, Micropor. Mesopor. Mater. 176 (2013) 78–85.
[34] X.R. Hu, G.L. Lu, Y. Yang, Determination of cation-exchange capacity in clay $[Co(NH_3)_{(6)}]^{(3+)}$ exchange method, Chin. J. Anal. Chem. 28 (2000) 1402–1405.
[35] L.Z. Zhu, R.L. Zhu, L.H. Xu, X.X. Ruan, Influence of clay charge densities and surfactant loading amount on the microstructure of CTMA-montmorillonite hybrids, Colloid Surf. A 304 (2007) 41–48.
[36] S.J. Gregg, K.S.W. Sing, Adsorption, Surface Area, and Porosity, 2nd ed., Academic Press, New York, 1982.
[37] R.S. Mikhail, S. Brunauer, E.E. Bodor, Investigations of a complete pore Structure Analysis. I. Analysis of Micropores, J. Colloid Interf. Sci. 26 (1968), 45-&.
[38] H.Y. Zhu, P. Cool, E.F. Vansant, Deriving pore size distributions of solids with both micro- and mesopores from comparison plots, Recent Adv. Sci. Technol. Zeolites Relat. Mater. Pts a–C 154 (2004) 1456–1463.
[39] J.P. Olivier, M.L. Occelli, Surface area and microporosity of a pillared interlayered clay (PILC) from a hybrid density functional theory (DFT) method, J. Phys. Chem. B 105 (2001) 623–629.
[40] X. Mo, D.E. Lopez, K. Suwannakarn, Y. Liu, E. Lotero, J.G. Goodwin, C.Q. Lu, Activation and deactivation characteristics of sulfonated carbon catalysts, J. Catal. 254 (2008) 332–338.
[41] P. Komadel, J. Madejová, Chapter 10.1—acid activation of clay minerals, in: B. Faïza, L. Gerhard (Eds.), Developments in Clay Science, Elsevier, 2013, pp. 385–409.
[42] J. Madejova, H. Palkova, M. Pentrak, P. Komadel, Near-infrared spectroscopic analysis of acid-treated organo-clays, Clay Clay Miner. 57 (2009) 392–403.
[43] M.A.V. Rodriguez, J.D.L. Gonzalez, M.A.B. Munoz, Influence of the free silica generated during acid activation of a sepiolite on the adsorbent and textural properties of the resulting solids, J. Mater. Chem. 5 (1995) 127–132.
[44] K.S.W. Sing, D.H. Everett, R.A.W. Haul, L. Moscou, R.A. Pierotti, J. Rouquerol, T. Siemieniewska, Reporting physisorption data for gas solid systems with special reference to the determination of surface-area and porosity (Recommendations 1984), Pure Appl. Chem. 57 (1985) 603–619.
[45] J. Pires, A.C. Araujo, A.P. Carvalho, M.L. Pinto, J.M. Gonzalez-Calbet, J. Ramirez-Castellanos, Porous materials from clays by the gallery template approach: synthesis, characterization and adsorption properties, Micropor. Mesopor. Mater. 73 (2004) 175–180.
[46] P. Yuan, D. Liu, M.D. Fan, D. Yang, R.L. Zhu, F. Ge, J.X. Zhu, H.P. He, Removal of hexavalent chromium [Cr(VI)] from aqueous solutions by the diatomite-supported/unsupported magnetite nanoparticles, J. Hazard. Mater. 173 (2010) 614–621.
[47] G. Jozefaciuk, C. Hoffmann, B. Marschner, Effect of extreme acid and alkali treatment on pore properties of soil samples, J. Plant Nutr. Soil Sci. 165 (2002) 59–66.
[48] H. Palkova, J. Madejova, M. Zimowska, E.M. Serwicka, Laponite-derived porous clay heterostructures: II. FTIR study of the structure evolution, Micropor. Mesopor. Mater. 127 (2010) 237–244.
[49] J. Madejova, J. Bujdak, M. Janek, P. Komadel, Comparative FT-IR study of structural modifications during acid treatment of dioctahedral smectites and hectorite, Spectrochim. Acta A 54 (1998) 1397–1406.
[50] J. Madejova, P. Komadel, Baseline studies of the clay minerals society source clays: infrared methods, Clay Clay Miner. 49 (2001) 410–432.
[51] M. Nocun, E. Leja, J. Jedlinski, J. Najman, Structure and optical properties of hybrid glasses based on tetraethylorthosilicate-trimethoxyoctylsilane and tetraethylorthosilicate-tetraethylorthotitanate-trimethoxyoctylsilane systems, J. Mol. Struct. 744 (2005) 597–602.
[52] Z. Olejniczak, M. Leczka, K. Cholewa-Kowalska, K. Wojtach, M. Rokita, W. Mozgawa, Si-29 MAS NMR and FTIR study of inorganic-organic hybrid gels, J. Mol. Struct. 744 (2005) 465–471.
[53] M.J. Webb, P. Palmgren, P. Pal, O. Karis, H. Grennberg, A simple method to produce almost perfect graphene on highly oriented pyrolytic graphite, Carbon 49 (2011) 3242–3249.
[54] A.P. Terzyk, The influence of activated carbon surface chemical composition on the adsorption of acetaminophen (paracetamol) in vitro Part II. TG, FTIR, and XPS analysis of carbons and the temperature dependence of adsorption kinetics at the neutral pH, Colloid Surf. A 177 (2001) 23–45.
[55] B. Wang, T.P. Ang, A. Borgna, A rapid hard template method for the synthesis of N-doped mesoporous carbon replicated from TUD-1, Micropor. Mesopor. Mater. 158 (2012) 99–107.
[56] J.R. Pels, F. Kapteijn, J.A. Moulijn, Q. Zhu, K.M. Thomas, Evolution of nitrogen functionalities in carbonaceous materials during pyrolysis, Carbon 33 (1995) 1641–1653.
[57] D.J. Malik, A.W. Trochimczuk, A. Jyo, W. Tylus, Synthesis and characterization of nanostructured carbons with controlled porosity prepared from sulfonated divinylbiphenyl copolymers, Carbon 46 (2008) 310–319.
[58] P. Valle-Vigon, M. Sevilla, A.B. Fuertes, Synthesis of uniform mesoporous carbon capsules by carbonization of organosilica nanospheres, Chem. Mater. 22 (2010) 2526–2533.
[59] D.D. Do, 6—heterogeneous adsorption equilibria, in: R.T. Yang (Ed.), Adsorption Analysis: Equilibria and Kinetics, Imperial College Press, London, 1998, pp. 249–336.
[60] M.A. Lillo-Rodenas, A.J. Fletcher, K.M. Thomas, D. Cazorla-Amoros, A. Linares-Solano, Competitive adsorption of a benzene-toluene mixture on activated carbons at low concentration, Carbon 44 (2006) 1455–1463.